

See discussions, stats, and author profiles for this publication at: <https://www.researchgate.net/publication/258500136>

Transferable Mixing of Atomistic and Coarse-Grained Water Models

ARTICLE *in* THE JOURNAL OF PHYSICAL CHEMISTRY B · NOVEMBER 2013

Impact Factor: 3.3 · DOI: 10.1021/jp4079579 · Source: PubMed

CITATIONS

16

READS

12

3 AUTHORS, INCLUDING:



[Leonardo Darre](#)

IRB Barcelona Institute for Research in Biom...

13 PUBLICATIONS 92 CITATIONS

[SEE PROFILE](#)



[Sergio Pantano](#)

Institut Pasteur de Montevideo

60 PUBLICATIONS 963 CITATIONS

[SEE PROFILE](#)

Transferable Mixing of Atomistic and Coarse-Grained Water Models

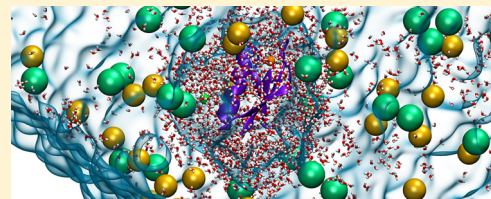
Humberto C. Gonzalez,[†] Leonardo Darré,^{†,‡} and Sergio Pantano^{*,†}

[†]Institut Pasteur de Montevideo, Mataojo 2020, Montevideo 11400, Uruguay

[‡]Department of Chemistry, King's College London, London, United Kingdom

Supporting Information

ABSTRACT: Dual-resolution approaches for molecular simulations combine the best of two worlds, providing atomic details in regions of interest and coarser but much faster descriptions of less-relevant parts of molecular systems. Given the abundance of water in biomolecular systems, reducing the computational cost of simulating bulk water without perturbing the solute's properties is a very attractive strategy. Here we show that the coarse-grained model for water called WatFour (WT4) can be combined with any of the three most used water models for atomistic simulations (SPC, TIP3P, and SPC/E) without modifying the characteristics of the atomistic solvent and solutes. The equivalence of fully atomistic and hybrid solvation approaches is assessed by comparative simulations of pure water, electrolyte solutions, and the β_1 domain of streptococcal protein G, for which comparisons between experimental and calculated chemical shifts at $^{13}\text{C}\alpha$ are equivalent.



INTRODUCTION

The high computational cost of molecular dynamics (MD) techniques motivates the development of time-saving strategies for simulations. As a consequence, different coarse-grained (CG) potentials reducing the number of particles and/or degrees of freedom of molecular systems have been developed to reach longer size and time scales.^{1–19} The expansion of different CG schemes to represent macromolecular entities has been naturally accompanied by the development of several models for aqueous solvation (recently reviewed in refs 20 and 21). In particular, our group has developed a CG water model inspired by the transient tetrahedral clusters formed by pure water, which is part of a set of CG parameters named SIRAH (www.sirahff.com). This CG water model, called WatFour (i.e., WT4), is composed of four beads interconnected in a tetrahedral conformation (Figure 1A,B) and achieves a good reproduction of several common properties of liquid water and simple electrolyte solutions.²² Because each bead carries an explicit partial charge, WT4 generates its own dielectric permittivity without the need to impose a uniform dielectric.

Despite the relatively good performance of CG models, there are situations in which atomistic detail cannot be neglected (e.g., those where hydrogen bonds play a determinant role). In those cases, hybrid or multiresolution schemes in which less-relevant parts of a molecular system treated on the CG level coexist with regions of interest treated on the fine-grain (FG) level of detail have been proposed using a large variety of approaches to couple regions treated at atomistic and supraatomic/molecular levels.^{23–35} Recently, we showed that it is possible to combine WT4 with the widely used SPC water model.³⁶ Simulations using pure FG and hybrid FG–CG solvation applied to a system containing simple electrolytes and a protein complex embedded in a double-membrane environment were shown to be equivalent up to statistical precision.³⁷ The underlying idea of this dual-resolution solvation scheme is

that at the FG level, solutes modify the structure and dynamics of neighboring water molecules.^{38,39} Charged or polar moieties act as pinning sites for water, forming an extended network of hydrogen bonds on the surface. Conversely, hydrophobic surfaces hamper the formation of water–water electrostatic interactions. Beyond proximal solvation shells, water recovers its bulk properties.⁴⁰ Therefore, a proper description of charged and polar moieties requires the explicit presence of fully atomistic water, but a high level of detail is less relevant for hydrophobic surfaces and bulk water. This suggests that a dual-resolution approach for solvent molecules around a macromolecule represents a suitable alternative to reducing the computational cost of molecular simulations with negligible effects on the structure and dynamics of the solute. For this hypothesis to be valid, the reciprocal free energies of solvation must determine a limited mixing of both solvents, spontaneously resulting in an FG–CG interface. An open question about this method regards its transferability because the free energies of solvation in WT4 change according to the interaction parameters of different FG water models. The relevance of this question resides in the fact that different force fields are fine tuned to work in combination with specific water models.⁴¹

Although a large variety of water models have been published (exhaustive compilation at <http://www.lsbu.ac.uk/water/models.html>), the simplest and most popular are those known as SPC,³⁶ TIP3P,⁴² and SPC/E.⁴³ Exhaustive testing on the compatibility of SPC-WT4 has been presented elsewhere³⁷ for systems containing pure water, electrolyte solutions, and a protein complex embedded in two parallel membrane bilayers. Therefore, in this work we focus on hybrid

Received: August 8, 2013

Revised: October 15, 2013

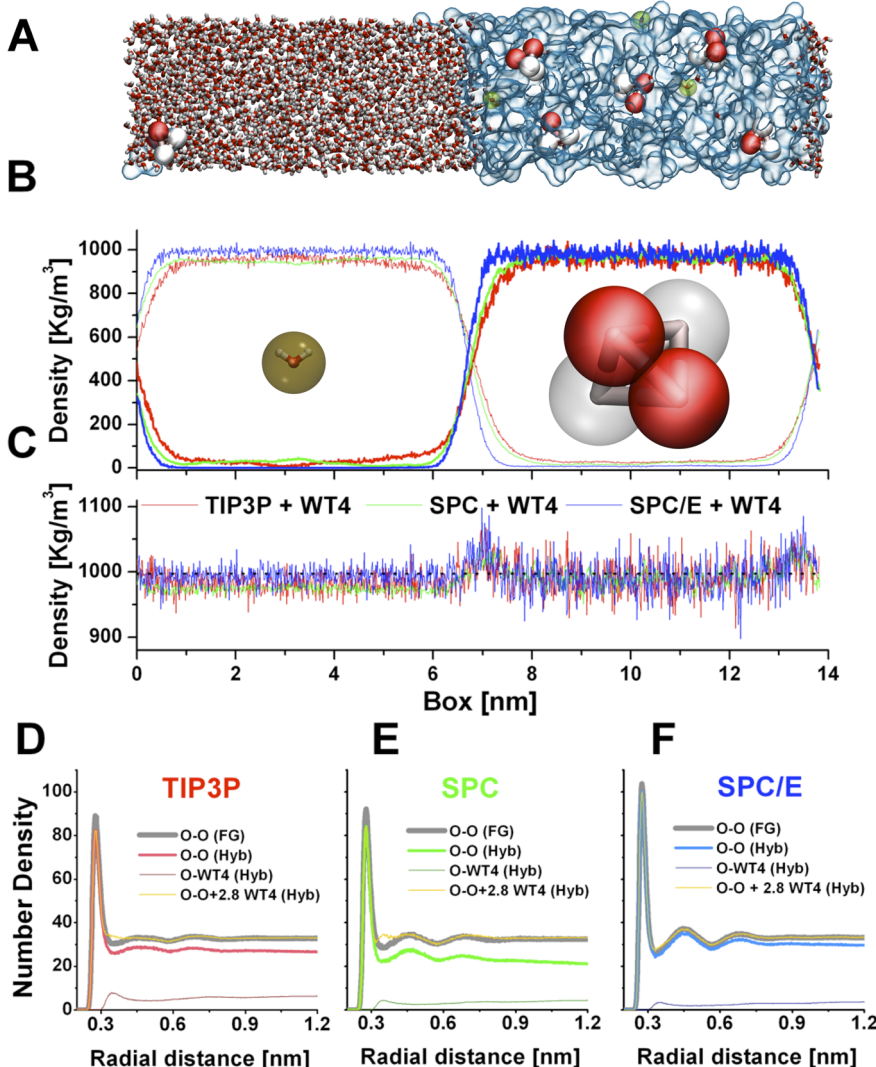


Figure 1. Pure water systems at hybrid resolution. (A) Snapshot of system 4 (Table 1, SPC/E-WT4) taken after 1 ns of MD simulation. FG water molecules are shown as sticks and colored by atom (red, oxygen; white, hydrogen). Systems using SPC and TIP3P are completely analogous and omitted for brevity. The CG region is represented by its solvent-accessible surface calculated with a probe radius of 0.14 nm (light blue). The vDW radii and connectivity of six WT4 molecules are shown to provide an idea of the molecular character of the CG phase. The vDW radius of three FG water molecules within the CG phase is shown in green to provide a visual comparison between the relative sizes of both solvents. (B) Water density profile calculated along the box axis perpendicular to the interface for the different molecular species in pure water systems. Thin and thick lines are used to indicate the densities of FG and CG systems, respectively. There is a rough correspondence between panels A and B. (C) Total density along the box calculated as the sum of the traces shown in panel B when considering that each WT4 bead corresponds to 2.8 water molecules. The dashed black line corresponds to the experimental value.⁵⁹ Oxygen–oxygen number densities of FG and CG species for systems containing (D) TIP3P, (E) SPC, and (F) SPC/E. Results in panel E are taken from ref 37. Thick gray traces are used for fully atomistic systems. Red and dark-red traces correspond to the number densities of TIP3P oxygen and WT4 beads, respectively. Green and dark-green traces correspond to SPC oxygen and WT4 beads, respectively. Blue and dark-blue traces correspond to SPC/E oxygen and WT4 beads, respectively. Yellow traces show the sum of FG oxygen plus 2.8 times of WT4 beads.

solvation using TIP3P and SPC/E, enlarging the range of applicability of our approach. The direct compatibility of WT4 with FG water models other than SPC is not obvious because SPC, TIP3P, and SPC/E display divergent thermodynamic properties for up to nearly 2-fold differences in self-diffusion, density maxima, and expansion coefficient.^{41,44} Here we show that despite minor differences our dual-resolution solvation approach using WT4 as supramolecular water is compatible with any of the above-mentioned FG water models. These results are validated by comparative simulations performed on pure water, simple electrolyte solutions, and the β_1 domain of streptococcal protein G,⁴⁵ used as a test case. Calculations of thermodynamic properties of liquids, global conformational

descriptors of proteins, and residue-level properties calculated along MD trajectories show essentially no differences, validating our hybrid solvation scheme.

COMPUTATIONAL DETAILS

All MD simulations are performed using the same protocol extensively described in ref 37. Briefly, we use the GROMACS 4.5 package⁴⁶ with a time step of 2 fs and a cutoff for nonbonded interactions of 1.2 nm, together with the particle mesh Ewald approach^{47,48} to evaluate long-range electrostatics. The LINCS algorithm⁴⁹ is applied to all bonds connecting hydrogen atoms, and SETTLE⁵⁰ is used for water models

Table 1. Simulated Systems

system number	system name	components and number of atoms (N.At.)	simulation time (ns)
1 ^a	pure SPC	SPC (4004), N.At. 12 012	5
2 ^a	hybrid SPC-WT4	SPC (2002), WT4 (182), N.At. 6734	5
3	pure SPC/E	SPC/E (4004), N.At. 12 012	15
4	hybrid SPC/E-WT4	SPC/E (2002), WT4 (182), N.At. 6734	15
5	pure TIP3P	TIP3P (4004), N.At. 12 012	15
6	hybrid TIP3P-WT4	TIP3P (2002), WT4 (182), N.At. 6734	15
7	SPC-WT4 interfacial tension	SPC(2447), WT4 (389), N.At. 8897	3
8	TIP3P-WT4 interfacial tension	TIP3P(2607), WT4 (361), N.At. 9265	3
9	SPC/E-WT4 interfacial tension	SPC/E(2447), WT4 (396), N.At. 8925	3
10 ^a	pure SPC ions	SPC(2002), Na ⁺ (10), Cl ⁻ (10), N.At. 6026	10
11 ^{a,b}	hybrid SPC-WT4 ions	SPC(2002), Na ⁺ (10), Cl ⁻ (10), WT4 (160), NaW ⁺ (10), ClW ⁻ (10), N.At. 6686	10
12	pure SPC/E ions	SPC/E(2002), Na ⁺ (10), Cl ⁻ (10), N.At. 6026	25
13 ^b	hybrid SPC/E-WT4 ions	SPC/E(2002), Na ⁺ (10), Cl ⁻ (10), WT4 (160), NaW ⁺ (10), ClW ⁻ (10), N.At. 6686	25
14	pure TIP3P-ions	TIP3P(2002), Na ⁺ (10), Cl ⁻ (10), N.At. 6026	25
15 ^b	hybrid TIP3P-WT4 ions	TIP3P(2002), Na ⁺ (10), Cl ⁻ (10), WT4 (160), NaW ⁺ (10), ClW ⁻ (10), N.At. 6686	25
16	protein-SPC/E	1FCL, SPC/E (55 717), Na ⁺ (50), Cl ⁻ (46), N.At. 168 113	30
17 ^b	protein-SPC/E WT4	1FCL, SPC/E (1422), Na ⁺ (2), Cl ⁻ (1), WT4 (4885), NaW ⁺ (48), ClW ⁻ (45), N.At. 24 768	30
18	protein-TIP3P	1FCL, TIP3P (55 717), Na ⁺ (50), Cl ⁻ (46), N.At. 168 113	30
19 ^b	protein-TIP3P WT4	1FCL, TIP3P (3065), Na ⁺ (2), Cl ⁻ (1), WT4 (4753), NaW ⁺ (48), ClW ⁻ (45), N.At. 29 169	30
20	hybrid SPC/E-WT4. CG ions on the FG side and vice versa	SPC/E(2002), Na ⁺ (10), Cl ⁻ (10), WT4 (160), NaW ⁺ (10), ClW ⁻ (10), N.At. 6686	30
21	hybrid TIP3P-WT4. CG ions on the FG side and vice versa	TIP3P(2002), Na ⁺ (10), Cl ⁻ (10), WT4 (160), NaW ⁺ (10), ClW ⁻ (10), N.At. 6686	30
22	protein-SPC/E	1FCL, SPC/E (3841), Na ⁺ (8), Cl ⁻ (4), N.At. 12 401	30
23	protein-SPC/E WT4	1FCL, TIP3P (1423), Na ⁺ (3), Cl ⁻ (1), WT4 (430), NaW ⁺ (5), ClW ⁻ (3), N.At. 6867	30
24	protein-TIP3P	1FCL, TIP3P (3841), Na ⁺ (8), Cl ⁻ (4), N.At. 12 401	30
25	protein-TIP3P WT4	1FCL, TIP3P (1423), Na ⁺ (3), Cl ⁻ (1), WT4 (430), NaW ⁺ (5), ClW ⁻ (3), N.At. 6867	30

^aTaken from ref 37. ^bNaW⁺ and ClW⁻ indicate CG ions.

(SPC, SPC/E, and TIP3P). Because of compatibility with our previous work,³⁷ the temperature and pressure are kept constant at 298 K and 1 atm using Berendsen thermostats and barostats,⁵¹ respectively. However, because this approach does not reproduce the correct energy distribution,⁵² we have performed an additional set of simulations for the same protein system using v-rescale⁵³ and Parrinello–Rahman⁵⁴ schemes. The results of these simulations performed using more rigorous temperature and pressure controls are essentially identical and are reported in the Supporting Information.

The relative free energies of solvation of the different water models using thermodynamic integration are calculated as reported elsewhere.³⁷ The calculation of the FG–CG water interfacial tension was done using a similar approach as used for the CG water surface tension,³⁷ substituting the vacuum-WT4 interface with the interface between each FG water model and WT4.

To assess the equivalence of pure FG and hybrid solvation on a protein solute, we simulate a variant of the β 1 domain of streptococcal protein G (PDB code 1FCL⁴⁵). The starting coordinates used for the MD simulations correspond to the first conformer of the NMR family of structures, which is reported as the best representative model. With the aim of mimicking the experimental conditions, we used a protein concentration of 1 mM with a NaCl concentration of 50 mM. This resulted in a relatively large solvation box. The molecular composition of the

simulated system is reported in Table 1. All of the systems undergo energy minimization and 1 ns of MD to achieve equilibration. Finally, 30 ns of plain MD simulations is performed for each system. With the aim of checking for transferability, we repeated the same simulation setup using AMBER99SB-ILDN⁵⁵ in combination with TIP3P and GROMOS⁵⁶ in combination and SPC/E, which includes a self-polarization energy correction⁴³ (Table 1).

All of the properties for systems 1 to 15 are calculated as previously described.³⁷ Root-mean-square deviations were calculated for the C α atoms of the proteins. Hydrogen bonds between side chains are considered to exist when the donor–acceptor distance between heavy atoms goes up to 0.35 nm and the hydrogen–donor–acceptor angle is smaller than 30°.

The number densities of solvent oxygen atoms around the protein are calculated after being centered on atoms O ϵ 1 and O ϵ 2 in Glu15, N ζ in Lys10, O γ 1 or C γ 2 in Thr16, and C δ 1 and C δ 2 in Leu12.

Differences between calculated and experimental chemical shifts at the ^{13}C α in the protein backbone (hereafter referred to as $\Delta\mu$) are estimated using the CheShift2 server⁵⁷ (<http://cheshift.com/>), which evaluates the deviation of chemical shift values from a distribution taken from a large set of experimental structures. Results are, therefore, expressed in terms of standard deviations from this reference distribution.⁵⁸ Amino acids having chemical shifts within two standard deviations from this

distribution are ascribed to good-quality conformations. In this work, $\Delta\mu$ are calculated on a set of 30 conformers taken at the end of each ns from the MD simulation.

RESULTS AND DISCUSSIONS

Pure Water. The underlying idea of our hybrid solvation method is that (as for any mixture of liquids) the differences in the reciprocal free energies of solvation of WT4 with a given atomistic solvent determine their propensity to mix. If both liquids undergo only partial mixing (Figure 1A), then they can coexist with minimal or no perturbation on the bulk physicochemical characteristics of each of the different components.

The free energies of solvation of the three atomistic models in WT4 and vice versa are reported in Table 2. The calculation

Table 2. Free Energies of Solvation of FG and Hybrid Models

solute	solvent	ΔG_{solv} (kJ mol ⁻¹)	$\Delta\Delta G$ (kJ mol ⁻¹)
WT4	SPC/E	-33.8	16.9 ^a
	SPC	-35.6	15.1 ^a
	TIP3P	-36.8	13.9 ^a
	WT4	-50.7	
SPC/E	WT4	-14.7	29.8 ^b
	SPC/E	-44.5	
SPC	WT4	-13.2	23.6 ^b
	SPC	-36.8	
TIP3P	WT4	-13.6	19.8 ^b
	TIP3P	-33.4	

^aCalculated as ΔG_{solv} (WT4 solute in FG solvent) - ΔG_{solv} (WT4 solute in WT4 solvent). ^bCalculated as ΔG_{solv} (FG solute in WT4 solvent) - ΔG_{solv} (FG solute in FG solvent).

of the differences between free energies of solvation, taking vacuum as the reference state ($\Delta\Delta G_{\text{solv}}$), suggests that the degree of mixing will be different for each model following the trend TIP3P > SPC > SPC/E. If simulations are performed on a computational box constructed with two apposed slabs of FG and CG water such as that shown in Figure 1A, then a limited number of molecules migrate from their own medium to the other.

Computing the density of each species along the simulation box results in two separated regions of alternating high and low densities of each water representation (FG and CG) with a sigmoidal transition (Figure 1B). Notably, if the total density is considered (i.e., summing FG and CG molecules), then the experimental value (on average) is retrieved in all cases (Figure

1C). Owing to the different granularity, the total density displays smaller oscillations in the FG region than in the CG counterpart, with an increase on the order of 5% at the interface. Stabilization of the densities is reached within the stabilization period (not shown), resulting in molar fractions of FG in CG molecules of 0.33, 0.28, and 0.11 for TIP3P, SPC and SPC/E, respectively.

The differences between $\Delta G_{\text{solv(}FG \text{ solute in FG solvent)}}$ are reflected in the steepness of the density change in the direction perpendicular to the FG-CG interface. TIP3P, SPC, and SPC/E models show progressively steeper interface regions (Figure 1B), in agreement with the higher stabilization energy yielded when solvating them in their own media (Table 2). This trend is also in agreement with the interfacial tension measured for each combination of FG and CG models (Table 3).

Besides the global density profiles, it is important to assess whether this hybrid solvation scheme perturbs the structural features of water. To address this point, we compare the number density distribution around FG water oxygen atoms. In line with the results obtained for SPC-WT4 solutions,³⁷ the distribution in each hybrid system shows a very good match to its respective FG counterparts (Figure 1D-F). This indicates that the CG water does not affect the solvation shells within the FG phase. An equivalent behavior is observed for the three water models, with small differences related to the intrinsic features of each FG solute. As the radial coordinate increases, the height of the function becomes underestimated for the hybrid solvation schemes as a result of the presence of the WT4 molecules. However, this difference is apparent and can be corrected by taking into account that each WT4 bead represents 2.8 FG water molecules (Figure 1D-F). The only noticeable difference resides in a slight decrease in the first solvation peak accompanied by the presence of a shallow shoulder between the first and second solvation shells. The cause of both effects is the presence of a few WT4 beads fleetingly contacting FG oxygen atoms during the simulation. This effect is slightly more pronounced in the cases of TIP3P and SPC (Figure 1D,E) owing to their higher tendency to mix with WT4, which increases the encounter probability between FG and CG particles. Accordingly, the use of SPC/E (Figure 1F), with the lowest degree of mixing, shows almost no traces of such an effect.

A wider and more comprehensive view of the performance of our solvation scheme can be acquired by contrasting some typical physicochemical properties resulting from FG and hybrid simulations (Table 3). In general, these comparisons result in rather small differences, especially considering the

Table 3. Comparison of Physicochemical Properties of Pure Water

	Kirkwood factor ^a	relaxation time ($\tau^{\text{HH}}_2/\tau^{\text{OH}}_2$) (ps)	relative permittivity	diffusion coefficient ($\times 10^{-5}$ cm ² s ⁻¹)	interfacial tension (mN/m) ^c
pure SPC	2.53	1.0/0.9	65	4.3	
hybrid SPC-WT4	2.9	1.2/1.0	84	2.9	8
pure SPC/E	2.69	1.9/1.7	75.5	2.55	
hybrid SPC/E-WT4	2.76	1.89/1.67	83.8	2.21	13
pure TIP3P	3.45	0.68/0.65	95	5.7	
hybrid TIP3P-WT4	3.33	0.69/0.66	100	4.1	6
pure WT4	^b	^b	110	2.23	
exp.	2.9 ^{41,60}	1.95 ⁶¹	78.5 ⁶²	2.27 ⁶³	

^aCalculated after 5 ns of simulation. ^bKirkwood factors and relaxation times cannot be calculated for WT4 molecules. ^cAs a reference, the experimental air-water surface tension is 71.2 mN/m and vacuum-WT4 is 17 mN/m.²²

differences existing between the FG water models and experimental values (Table 3).

Kirkwood factors, which are a measure of the dipole–dipole correlation between solvent molecules, give a maximum difference of about 15% when WT4 is mixed with SPC, whereas the difference with FG systems is about 4% for SPC/E and TIP3P (Table 3). Similarly, the relaxation or tumbling times (i.e., the time needed for a water molecule to rotate a radian within a certain medium) indicates that the highest difference is obtained for SPC whereas the agreement with the other two models is very good.

The evaluation of the dielectric permittivity and diffusion coefficients shows the same trend. The SPC model presents the highest deviation from its pure FG counterpart, whereas TIP3P and SPC/E present smaller deviations from the FG values (Table 3).

Taken together, these data suggest that our hybrid scheme of solvation is compatible with the use of the three FG models analyzed. Moreover, the differences between hybrid and homogeneous liquids are smaller than those existing between atomistic models themselves.

Electrolytic Solutions. Simulations with free electrolytes are carried out for both SPC/E and TIP3P in hybrid solvation schemes. The concentration of NaCl is set to 0.3 M in both phases. In the case of the CG region, we use the CG ions previously developed by us.²² As can be observed from the averaged density along the direction perpendicular to the interface, FG and CG electrolytes show a marked tendency to remain in their own region (Figure 2A,B). It is also clear from

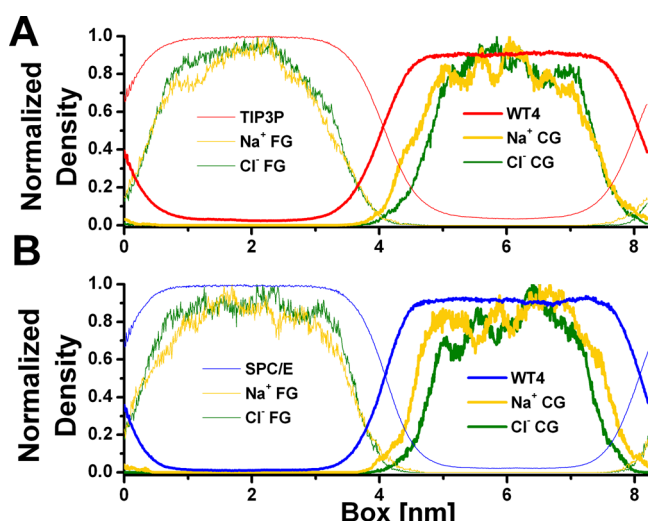


Figure 2. Electrolyte solutions and hybrid representation. (A) Normalized density profiles along the box axis perpendicular to the interface for a system containing TIP3P water as the FG solvent. Thin and thick lines are used to indicate the densities of FG and CG systems, respectively. (B) Idem to A for a system containing SPC/E water as the FG solute.

Figure 2 that the electrolyte density profiles show higher fluctuations when compared to the water density. This is derived from the relatively reduced number of electrolytes considered (Table 1). Notably, the presence of the interface creates a region depleted of electrolytes because ionic species need a minimal solvation shell to achieve good electrostatic stabilization. This effect is more marked in the bulkier CG chloride ions, which remain more separated from the middle of

the box. In contrast to water molecules, which experience limited mixing, the density of FG ions decreases to zero in the CG phase and vice versa, indicating that all electrolytes remain within their respective phases for the entire simulation time. In setting up these systems, FG and CG water molecules were substituted with their corresponding species-specific electrolytes. Therefore, there is the possibility that ions remain kinetically trapped in their media during the relatively limited simulation time. To rule out this possibility, we prepared systems in which FG ions were positioned in the CG region and vice versa. Using this starting configuration, electrolytes partition in their own solvent region within 2 ns (see animations at <http://www.youtube.com/watch?v=Mw1qBj9w5uM>). This rapid exchange supports the idea that the localization of ions in their own medium results from an unfavorable energy change in moving an ion from a given resolution into the bulk of the other. Unfortunately, this kind of calculation for charged species requires the inclusion of counterions or a uniform neutralizing background, both of which introduce spurious effects that are difficult to evaluate. This leads to large uncertainties that preclude the possibility of a precise estimation of the free energy of solvation for ionic species.⁶⁴

The hybrid scheme has only modest effects on the diffusion coefficient of the different electrolytes (Table 4). In correspondence with the case of pure water, the differences observed between the FG and hybrid simulations are always smaller than the differences existing between the FG models themselves.

Protein Systems. By considering the results obtained for pure water and free electrolytes in aqueous solution, it can be expected that the dual solvation scheme proposed here may be useful in speeding up simulations in biologically relevant systems. To evaluate the performance of pure FG and hybrid solvation, we undertook the simulation of the β 1 domain of streptococcal protein G⁴⁵ (PDB code 1FCL) using FG and FG–CG solvation approaches. This protein was considered to be a suitable test case because it contains the most common secondary structural motifs stabilized by hydrogen bonds (one α helix and four β strands forming parallel and antiparallel sheets, Figure 3A). Furthermore, experimental chemical shifts are deposited at the BMRDB (<http://www.bmrb.wisc.edu/>) with accession code S152, allowing for a stringent evaluation of the quality of local structural determinants.

Because our aim was to determine the transferability of our solvation scheme, we performed simulations using the same protein structure and two different force fields. A comparison is made in each case between the FG and hybrid solvation schemes. An exhaustive analysis of the performance of hybrid SPC–WT4 solvation against pure SPC has recently been presented elsewhere;³⁷ therefore, we will limit the discussion of the results in this section to systems simulated using AMBER and GROMOS solvated with TIP3P and SPC/E, respectively.

In our previous work, hybrid systems were constructed by solvating the solute with a 1-nm-thick SPC water shell. Then, WT4 molecules were added to fill the computational box. Ions can be added by randomly substituting solvent molecules to match the desired ionic strength in the FG and CG regions of the system. However, to establish a general rule, it is necessary to take into account that the molar fractions at the equilibrium of the different FG water models result in diverse degrees of mixing (Figure 1B). Therefore, to keep the transferability of the hybrid approach and establish a one-to-one comparison

Table 4. Comparison of Diffusion Coefficients of Free Electrolytes in Aqueous Solutions

	Na ⁺ diffusion coefficient ($\times 10^{-5}$ cm ² s ⁻¹)			Cl ⁻ diffusion coefficient ($\times 10^{-5}$ cm ² s ⁻¹)		
	SPC	SPC/E	TIP3P	SPC	SPC/E	TIP3P
FG	2.2 ± 0.1	0.8 ± 0.1	2.1 ± 0.4	2.3 ± 0.3	1.5 ± 0.1	3.2 ± 0.2
hybrid	1.1 ± 0.2	0.8 ± 0.5	1.5 ± 0.1	1.8 ± 0.1	1.2 ± 0.2	2.7 ± 0.5
exp.		1.35 ± 0.038 ^a			1.91 ± 0.025 ^b	

^aNa⁺Cl⁻ concentration: 0.3 M.⁶⁵ ^bNa⁺Cl⁻ concentration: 0.25 M.⁶⁶

between simulations using different force fields and water models, it is necessary to solvate the FG region using premixed water boxes. These water boxes can be extracted from the CG region of the simulations of systems 2, 4, and 6 (Table 1) for SPC, SPC/E, and TIP3P, respectively. From the above-quoted molar fractions, we derived as a practical rule that hybrid solvation boxes must contain 3, 4, or 10 WT4 molecules per each TIP3P, SPC, or SPC/E, respectively. Therefore, we first solvated the proteins with a 1 nm shell of FG water and eventually substituted water from that shell with FG ions. This FG droplet is then solvated with prestabilized hybrid water boxes. Finally, CG ions are added to the solution by substituting WT4 molecules, yielding systems 17, 19, 23, and 25.

It is important to notice that a FG region surrounded by an interface of CG particles will produce a finite interfacial tension, increasing the pressure within the FG drop. In the macroscopic limit, this change in pressure across the interface can be described by the Young–Laplace equation as $\Delta p = 2\gamma/r$, where γ is the interfacial tension and r is the radius of the cavity. This clearly implies a divergence of the inner pressure when r approaches zero. Therefore, for highly curved systems with radial dimensions comparable to those of the molecular constituents, a correction was proposed by Tolman to take into account the change in the interfacial tension as a function of the radius of the cavity.⁶⁷ In our case the, surface tension changes according to $\gamma_{\text{eff}} = \gamma(1 - \delta/r)$, where γ_{eff} is the effective interfacial tension at the curved interface, γ is the interfacial tension on a plane, δ is the so-called Tolman length, which can be considered to be the thickness of the interface, and r is the radius of the droplet. There is a current debate on the precise definition of the Tolman length (e.g., refs 68 and 69 and references therein) that goes far beyond the scope of this work. For what concerns the present contribution, we are interested in a rough estimation of the pressure within a FG drop and whether it can appreciably distort the conformation of a folded protein. As a first approximation, it can be considered that the radius of the droplet corresponds to the radius of gyration of any protein plus 1 nm of FG water. The interfacial tension for each FG water model is reported in Table 3, and the Tolman length can be estimated from Figure 1B as ~1 nm in all cases. The use of these rough values for hybrid systems containing SPC/E, SPC, and TIP3P models on the above equations results in maximal pressures of 6.5, 4, and 3 bar, respectively, for a protein radius of gyration of 1 nm. Larger protein sizes result in smaller values (Figure SI 1). Therefore, it is important to determine if this excess pressure intrinsic to the hybrid solvation scheme can affect the structure or dynamics of the FG region, as discussed in the next sections.

Solvation Structure. Before comparing the structural/dynamical characteristics of each simulation, we assess the correct reproduction of the local solvation structure in the surroundings of amino acids with different physical/chemical characteristics. To this aim, we select five different atom types

belonging to different amino acids taken as a representative set. A direct comparison is always made with a simulation performed at the FG level (systems 16 and 18 in Table 1). Moreover, analogous simulations are performed using different thermostats and barostats (systems 22 to 25 in Table 1). These results are reported in the Supporting Information (Figures SI 2 to 5). For hydrophilic interactions, we selected three representative side-chain moieties, namely, oxygen atoms O ϵ of Glu15, the nitrogen (N ζ) at the side chain of Lys10, and oxygen O γ of Thr16 (Figure 3A).

For simulations performed using AMBER-TIP3P, the radial distribution of solvent around Glu15 reproduced by the hybrid approach shows very good correspondence with the fully atomistic counterpart. Within a radial distance of ~0.6 nm, the FG water in the hybrid simulation is superimposed with that of the homogeneous system including the first and second solvation shells (Figure 3B). Only after that point does the amount of CG water reach a significant level and increase continuously toward the bulk region. As observed for pure water (Figure 1D), adding both distributions in the hybrid simulation and taking into account that each WT4 represents 2.8 water molecules results in a good matching of the FG curve in all of the surrounding space. An evaluation of the same property on the amine moiety of Lys10 provides essentially the same picture (Figure 3C), suggesting good performance of the hybrid approach despite the differences in the solvation structure imposed by positive and negative charges. Next, we focus on a more challenging situation, the side chain of Thr16, which is taken as a representative amphipathic moiety. As depicted in Figure 3D, the reproduction of the solvent profile around O γ in Thr16 is also very good within the first and second solvation shells. Only a small underestimation in relation to the FG density is observed at a radial distance of between 0.7 and 0.9 nm.

To characterize the solvent organization around hydrophobic moieties, we choose the carbons at positions γ in Thr16 and δ in Leu12. In the first case, the global reproduction of the hydrophobic profile (Figure 3E) shows the same features found for O γ in Thr16. It is likely that this effect is related to the amphipathic character of this amino acid, and the close proximity between the hydroxyl and methyl moieties at position γ may present some challenges for the hybrid approach. In support of this hypothesis, the radial distribution around the methyl groups at the δ position in Leu12 shows a better match with the full FG simulation (Figure 3F). Overall, these results suggest that the FG phase is not significantly perturbed by the CG region when using AMBER-TIP3P parameters.

The simulation of the same protein system using the GROMOS force field and SPC/E water in combination with WT4 revealed some unexpected features. Although we generally obtain good agreement with FG simulations, in this case WT4 beads come closer to the solute than they do with AMBER-TIP3P. Instead of a smooth sigmoidal growth of the

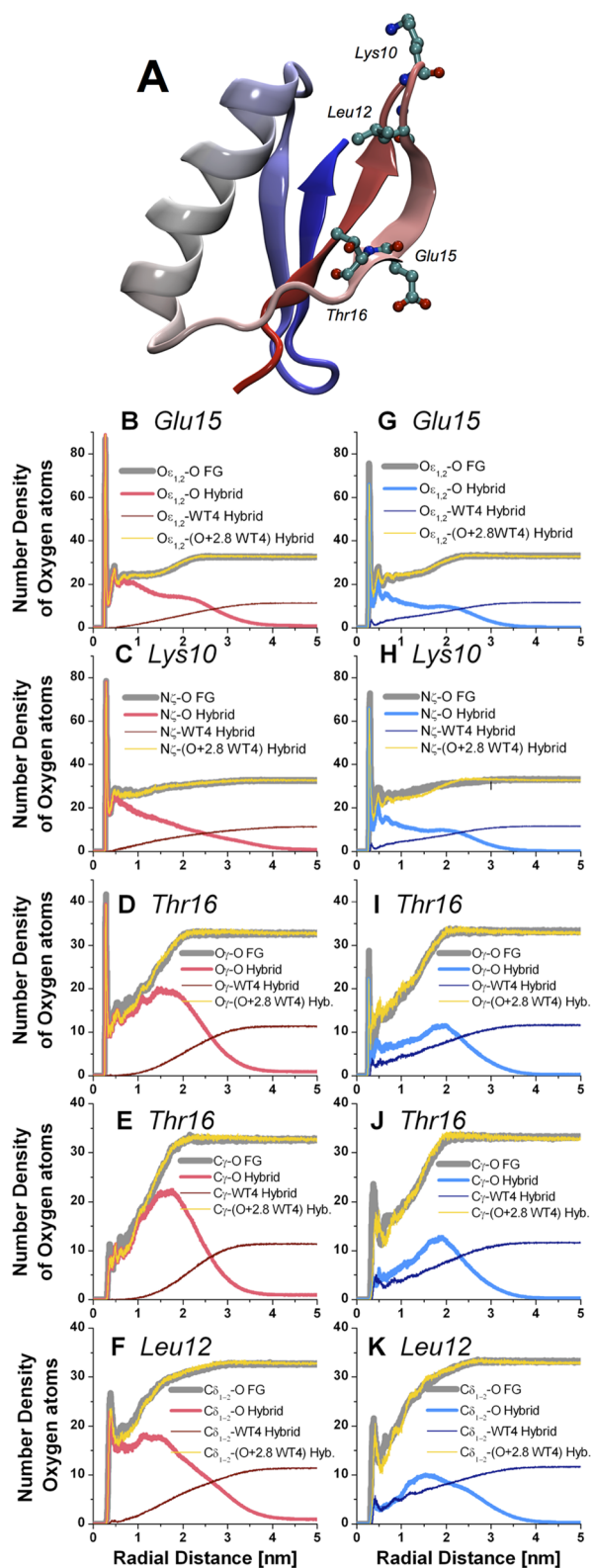


Figure 3. Solvation structure around FG amino acids. (A) Cartoon representation of the $\beta 1$ domain of streptococcal protein G (PDB id 1FCL). Colors go from red for the N terminal to blue for the C terminal. Residues used to calculate the solvent structure are presented as balls and sticks and are colored by atom. (B–F) Number densities of oxygen atoms around representative residues using AMBER-TIP3P parameters. (G–K) Same as in B–F using GROMOS-SPC/E parameters. Colors in panels B–K are the same as in Figure 1.

CG solvent density (WT4 traces in Figure 3B–F), a shallow peak of WT4 is present in close proximity to the solute (WT4 traces in Figure 3G–K). This is somehow surprising given the steepness of the FG–CG interface (Figure 1B) and the differences in solvation energies calculated for SPC/E and WT4 (Table 2). Hence, this behavior can likely be ascribed to specific protein–WT4 interactions resulting from the two force fields used. Nevertheless, the global results of the hybrid simulation (i.e., the equivalent number of solvent particles around the selected amino acids) are still comparable to the full FG cases. Moreover, these do not seem to influence the structure or dynamics of the protein solute (see below).

Recently, Riniker and co-workers reported that a similar solvation scheme using another CG model to represent supramolecular water may result in increased formation of intramolecular hydrogen bonds, especially between side chains.^{34,70} Therefore and in view of the observation of the changes in the solvation structure with the force field, we checked the occurrence of hydrogen bonds along the trajectories. The calculation of the inter-side-chain hydrogen bonds along the trajectories results in similar distributions for all the cases. Mean values and deviations calculated along the global distributions indicate that intrinsic variations are on the order of one hydrogen bond (Figure 4).

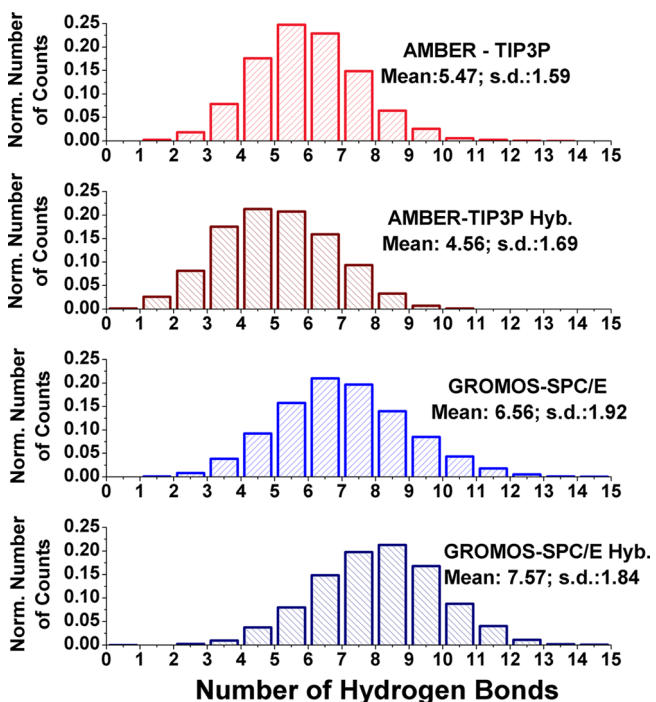


Figure 4. Inter-side-chain hydrogen bonds. Distribution of the normalized number of hydrogen bonds for FG (light red or blue) and hybrid (dark red or blue) simulations using AMBER-TIP3P (top) and GROMOS-SPC/E (bottom). Mean values and standard deviation of each distribution are reported on the corresponding panels.

The hybrid simulation based on the AMBER-TIP3P parameters shows a slightly reduced number of inter-side-chain hydrogen bonds when compared to its FG counterpart, whereas the opposite behavior is observed when using GROMOS-SPC/E (Figure 4). However, a comparison of average values and standard deviations indicates that the distributions of FG and hybrid solvation are indeed statistically equivalent.

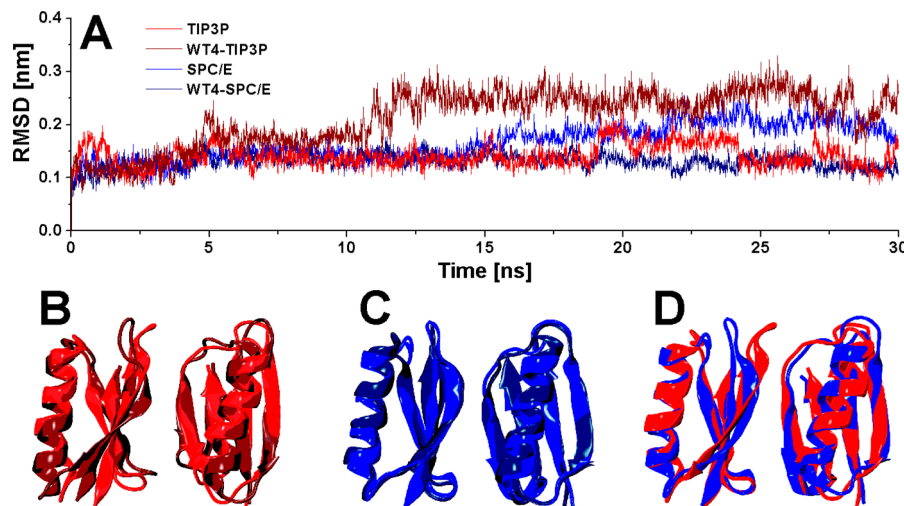


Figure 5. Structural comparison of protein simulations with different force fields and solvation approaches. (A) rmsd calculated over the Ca atoms. Light and dark colors are used to indicate FG and hybrid solvation schemes, respectively. (B) Structural superposition of the final FG and hybrid conformers after 30 ns of simulation performed using AMBER-TIP3P. The two panels correspond to the same superposition rotated 90° along the vertical axis. (C) Same as in B for the simulations performed using GROMOS-SPC/E. (D) Same as in B for final conformers from FG simulations using both force fields and water models.

Impact of Hybrid Solvation on Protein Conformation. Clearly, it is necessary to evaluate the impact of the dual-resolution solvation on the protein structure and dynamics. Moreover, it is important to appraise if the combination of FG–CG solvents is suitable for both force fields used. In all cases, the global folding of the protein is well maintained as suggested by the traces of rmsd versus time (Figure 5A). Within the first 10 ns, all of the traces are nearly equivalent. However, the conformation of the proteins simulated using the AMBER force field and the hybrid solvation scheme suffers an increase of about 0.05 nm in rmsd after that time and continues to oscillate around 0.26 nm. The FG simulation performed with AMBER-TIP3P undergoes transient increases in rmsd at the beginning of the simulation, between 18 and 24 ns, and toward the end of the time window explored. However, the FG simulation using GROMOS-SPC/E presents a smooth rise after 15 ns, whereas its hybrid counterpart stabilizes, rapidly oscillating around 0.12 nm for the entire simulation time (Figure 5A).

Taken together, the rmsd deviations are within the typical range of variation expected for any series of FG simulations. The structural superposition of final conformers suggests that the larger differences are, not surprisingly, in the loopy regions of the protein (Figure 5B,C) and that the differences observed are compatible with those existing between fully atomistic simulations using different force fields (Figure 5D).

With the aim of supporting this conclusion, we sought to assess the similarity between the conformational spaces sampled by the two simulations. Hence, we calculated and diagonalized the covariance matrixes of the Ca carbons along the simulations. This gives a total of 168 eigenvectors, and among those we selected the first 25, whose cumulative sum accounts for more than 80% of the variance in any of the 4 simulations carried out. We then calculated the overlap between this set of vectors between the fully atomistic and hybrid simulations using the same force field. As a reference, we calculated the overlap between the first 25 eigenvectors of the 2 fully atomistic systems (Table 5). It turns out that in both cases the subspace described by the set of 25 vectors overlaps by

Table 5. Overlap and Cumulative Variance Calculated for the First 25 Eigenvectors of the Covariance Matrixes

overlap	eigenvalue sum (FG)	eigenvalue sum (hybrid)
GROMOS-SPC/E (FG) vs GROMOS-SPC/E (Hybrid)		
74.1%	89%	84%
AMBER-TIP3P (FG) vs AMBER-TIP3P (Hybrid)		
75.6%	89%	82%
GROMOS-SPC/E (FG) vs AMBER-TIP3P (FG)		
67.4%	89%	89%

nearly 75%. Notably, the degree of superposition between both fully atomistic simulations is smaller than that obtained for FG and the hybrid. This suggests that although both solvation approaches may not be exactly equivalent, the differences between the subspaces sampled by simulations using different force fields are more relevant than those introduced by our solvation scheme.

The integration of the results of the previous paragraphs underlines the similarity between both solvation approaches. These results, however, are based on global descriptors, which may hide local flaws in the amino acid's conformations. In particular, this may raise the reasonable concern that loop conformations, which are the most different regions between both simulations, may sample unfavored configurations.

To rule out this possibility, we calculated the differences between the observed and predicted chemical shifts of the $^{13}\text{C}\alpha$ carbons ($\Delta\mu$). This quantity constitutes a stringent test for local structural deviations, being sensitive to distortions in the backbone and side-chain conformations.⁷¹ Mapping of the calculated $\Delta\mu$ along both hybrid simulations onto the final conformer of each trajectory indicates that the conformations sampled by each amino acid are in good agreement with experimental data (Figure 6A). However, a quantitative comparison between $\Delta\mu$ calculated on the FG and hybrid simulations underlines the equivalence between both solvation approaches (Figure 6B). The confidence intervals for the $\Delta\mu$ of the amino acids in the FG solvation scheme show good overlap with their hybrid counterparts in both force fields used. This is true for all of the amino acids using both force fields but for

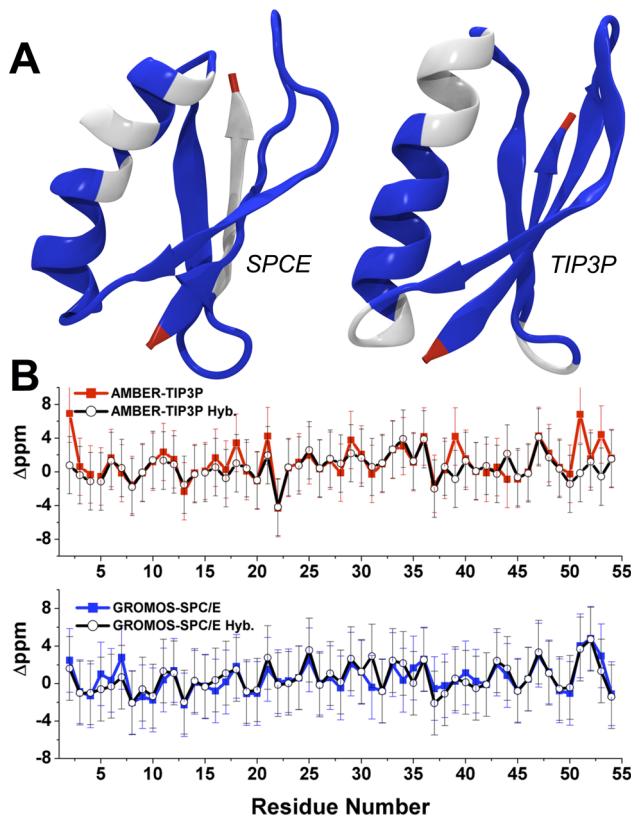


Figure 6. Local structural validation against NMR data. (A) Mapping of $\Delta\mu$ on final conformers of hybrid solvent simulations. Amino acids are colored blue or white if they deviate one or two standard deviations from expected values.⁵⁸ N and C termini, for which the calculation of $\Delta\mu$ is not possible, are colored red. (B) Comparison between $\Delta\mu$ calculated using FG and hybrid solvents. Error bars are set to 3.4 ppm according to the criterion of good-quality conformations.⁵⁷

Thr51 in the AMBER-TIP3P simulation, which shows statistically different $\Delta\mu$ in FG and hybrid simulations. Nevertheless, the difference between the confidence intervals is less than 0.5 ppm, which may be compatible with the line widths expected for typical ^{13}C signals.⁷²

CONCLUSIONS

Increasing effort is being devoted by the scientific community to developing CG representations of macromolecules that allow for faster and more accurate descriptions of interactions ruling biological or physical/chemical processes. Because water occupies a central position in this scenario, hybrid MD simulations offer the great potential of achieving a substantial reduction of computational cost without compromising accuracy. A number of highly efficient CG models for water have been developed recently,^{20,21} and some of them have been implemented as a part of dual-resolution solvents.^{30,34,37} However, the transferability of CG models to different FG force fields has not yet been explored, despite its practical relevance. In this work, we present a comparative study of the performance of the WT4 model when mixed with TIP3P and SPC/E water models and their commonly associated force fields for proteins. This adds to our previous work centered on a hybrid solvent using WT4 and SPC water,³⁷ completing the set of the most widely used FG models. The mixing propensity of each water model with WT4 is slightly different, resulting in

progressively smoother FG–CG interfaces for TIP3P, SPC, and SPC/E, thus modifying the interfacial tension of each FG–CG mixture. Nevertheless, common physical/chemical properties of FG water and simple electrolyte solutions are not significantly affected by the dual-solvation scheme. Simulations of a protein embedded in a hybrid solvent resulted in statistically equivalent structural and dynamical descriptions for both approaches. Similar results have recently been reported by Riniker et al. for a different CG model in combination with SPC water and using a different CG model.⁷³ In that case, a 0.8 nm water layer is found to be sufficient to ensure good compatibility with atomistic simulations.⁷⁰ Despite the variation in the CG model used and differences in the practical implementation (mainly, the use of restraints to hold water in the solute neighborhood and the reaction field for electrostatics used by Riniker et al. in comparison to PME and the absence of restraints in our case), both approaches may be considered to be roughly equivalent.

An important but previously overlooked issue of hybrid solvation schemes regards the increment of the internal pressure within the FG bubble because of the presence of the FG–CG interface. The rough estimation carried out here indicates that combining SPC/E with WT4 can artificially increase the pressure exerted on a small protein up to 6.5 times, as for the one studied here, whereas TIP3P and SPC water models result in smaller values. However, this does not seem to translate in spurious effects in the structure or dynamics of the protein. Moreover, the radii of gyration remain practically unchanged along the different simulations performed (Figure SI 5A). This may not be surprising considering (i) the much larger fluctuations produced by the barostats used in MD simulations and (ii) the fact that much larger pressures are needed to unfold proteins.⁷⁴ A different scenario can be expected for unfolded macromolecules, which may be more sensitive to external pressure.

Finally, it is clear that the increase in computational speed of this kind of method depends mainly on the total number of FG particles that can be substituted by CG molecules and also on the simulation program and hardware used. Considering the systems and setup used here, we can estimate that substituting 50% of the FG water results in ~2-fold acceleration, which can increase to about 5-fold for large solvation boxes that closely represent NMR experimental concentrations (Figure SI 6). It is noteworthy that this gain comes at a minimal cost in accuracy. The implementation of multiple time step algorithms and the improvement of current domain decomposition strategies for inhomogeneous systems in MD packages⁷⁵ will certainly boost hybrid approaches in the near future.

ASSOCIATED CONTENT

Supporting Information

Variation of the inner pressure as a function of the radius of the FG drop. Results of fully atomistic and hybrid solvation performed with a v-rescale thermostat and a Parrinello–Rahman barostat. Radii of gyration of the proteins along MD simulations. Speed-up of simulation as a function of the ratio between FG and CG water molecules. This material is available free of charge via the Internet at <http://pubs.acs.org>.

AUTHOR INFORMATION

Corresponding Author

*Tel: +598-2522 0910. Fax: +598-2522 0910. E-mail: spantano@pasteur.edu.uy.

Notes

The authors declare no competing financial interest.

ACKNOWLEDGMENTS

This work was partially supported by ANII- Agencia Nacional de Investigación e Innovación, Programa de Apoyo Sectorial a la Estrategia Nacional de Innovación-INNOVA URUGUAY (agreement n8 DCI – ALA/2007/19.040 between Uruguay and the European Commission). H.C.G. is the beneficiary of a fellowship from CSIC Uruguay.

REFERENCES

- (1) Voth, G. A. *Coarse-Graining of Condensed Phase and Biomolecular Systems*; Taylor & Francis Group: New York, 2009.
- (2) Marrink, S. J.; Risselada, H. J.; Yefimov, S.; Tieleman, D. P.; De Vries, A. H. The Martini Force Field: Coarse Grained Model for Biomolecular Simulations. *J. Phys. Chem. B* **2007**, *111*, 7812–7824.
- (3) Nielsen, S. O.; Lopez, C. F.; Goundla, S.; Klein, M. L. Coarse Grain Models and the Computer Simulation of Soft Materials. *J. Phys.: Condens. Matter* **2004**, *16*, R418.
- (4) Tozzini, V. Coarse-Grained Models for Proteins. *Curr. Opin. Struct. Biol.* **2005**, *15*, 144–150.
- (5) Chebaro, Y.; Pasquali, S.; Derreumaux, P. The Coarse-Grained Opep Force Field for Non-Amyloid and Amyloid Proteins. *J. Phys. Chem. B* **2012**, *116*, 8741–8752.
- (6) Onuchic, J. N.; Wolynes, P. G. Theory of Protein Folding. *Curr. Opin. Struct. Biol.* **2004**, *14*, 70–75.
- (7) Orsi, M.; Essex, J. W. The Elba Force Field for Coarse-Grain Modeling of Lipid Membranes. *PLOS One* **2011**, *6*, E28637.
- (8) Sansom, M. S.; Scott, K. A.; Bond, P. J. Coarse-Grained Simulation: A High-Throughput Computational Approach to Membrane Proteins. *Biochem. Soc. Trans.* **2008**, *36*, 27–32.
- (9) Murtola, T.; Bunker, A.; Vattulainen, I.; Deserno, M.; Karttunen, M. Multiscale Modeling of Emergent Materials: Biological and Soft Matter. *Phys. Chem. Chem. Phys.* **2009**, *11*, 1869–1892.
- (10) Bereau, T.; Deserno, M. Generic Coarse-Grained Model for Protein Folding and Aggregation. *J. Chem. Phys.* **2009**, *130*, 235106.
- (11) Potoyan, D. A.; Savelyev, A.; Papoian, G. A. Recent Successes in Coarse-Grained Modeling of DNA. *WIREs Comput. Mol. Sci.* **2013**, *3*, 69–83.
- (12) Dans, P. D.; Zeida, A.; Machado, M. R.; Pantano, S. A Coarse Grained Model for Atomic-Detailed DNA Simulations with Explicit Electrostatics. *J. Chem. Theory. Comput.* **2010**, *6*, 1711–1725.
- (13) Knotts, T. A.; Rathore, N.; Schwartz, D. C.; De Pablo, J. J. A Coarse Grain Model for DNA. *J. Chem. Phys.* **2007**, *126*, 084901.
- (14) Basdevant, N.; Borgis, D.; Ha-Duong, T. Modeling Protein–protein Recognition in Solution Using the Coarse-Grained Force Field Scorpion. *J. Chem. Theor. Comput.* **2013**, *9*, 803–813.
- (15) Ruhle, V.; Junghans, A.; Lukyanov, A.; Kremer, K.; Andrienko, D. Versatile Object-Oriented Toolkit for Coarse-Graining Applications. *J. Chem. Theor. Comput.* **2009**, *5*, 3211–3223.
- (16) Riniker, S.; Allison, J. R.; Van Gunsteren, W. F. On Developing Coarse-Grained Models for Biomolecular Simulation: A Review. *Phys. Chem. Chem. Phys.* **2012**, *14*, 12423–12430.
- (17) Ingolfsson, H. I.; Lopez, C. A.; Uusitalo, J. J.; De Jong, D. H.; Gopal, S. M.; Periole, X.; Marrink, S. J. The Power of Coarse Graining in Biomolecular Simulations. *WIREs Comput. Mol. Sci.* **2013**, DOI: 10.1002/Wcms.1169.
- (18) Cagnolini, T.; Derreumaux, P.; Pasquali, S. Coarse-Grained Simulations of RNA and DNA Duplexes. *J. Phys. Chem. B* **2013**, *117*, 8047–8060.
- (19) Dans, P. D.; Darré, L.; Machado, M. R.; Zeida, A.; Brandner, A. F.; Pantano, S. Assessing the Accuracy of the Sirah Force Field to Model DNA at Coarse Grain Level. In *Advances in Bioinformatics and Computational Biology*; Setubal, J. C., Almeida, N. F., Eds.; Springer International Publishing: New York, 2013; pp 71–81.
- (20) Hadley, K. R.; McCabe, C. Coarse-Grained Molecular Models of Water: A Review. *Mol. Simul.* **2012**, *38*, 671–681.
- (21) Darré, L.; Machado, M. R.; Pantano, S. Coarse Grain Models of Water. *WIREs Comput. Mol. Sci.* **2012**, DOI: 10.1002/Wcms.1097.
- (22) Darré, L.; Machado, M. R.; Dans, P. D.; Herrera, F. E.; Pantano, S. Another Coarse Grain Model for Aqueous Solvation: Wat Four? *J. Chem. Theory. Comput.* **2010**, *6*, 3793–3807.
- (23) Machado, M. R.; Dans, P. D.; Pantano, S. A Hybrid All-Atom/Coarse Grain Model for Multiscale Simulations of DNA. *Phys. Chem. Chem. Phys.* **2011**, *13*, 18134–18144.
- (24) Shi, Q.; Izvekov, S.; Voth, G. A. Mixed Atomistic and Coarse-Grained Molecular Dynamics: Simulation of a Membrane-Bound Ion Channel. *J. Phys. Chem. B* **2006**, *110*, 15045–15048.
- (25) Abrams, C. F.; Delle, S. L.; Kremer, K. Dual-Resolution Coarse-Grained Simulation of the Bisphenol-A-Polycarbonate/Nickel Interface. *Phys. Rev. E* **2003**, *67*, 021807.
- (26) Praprotnik, M.; Delle, S. L.; Kremer, K. Adaptive Resolution Molecular-Dynamics Simulation: Changing the Degrees of Freedom on the Fly. *J. Chem. Phys.* **2005**, *123*, 224106–224120.
- (27) Orsi, M.; Noro, M. G.; Essex, J. W. Dual-Resolution Molecular Dynamics Simulation of Antimicrobials in Biomembranes. *J. R. Soc., Interface* **2011**, *8*, 826–841.
- (28) Di Pasquale, N.; Marchisio, D.; Carbone, P. Mixing Atoms and Coarse-Grained Beads in Modelling Polymer Melts. *J. Chem. Phys.* **2012**, *137*, 164111.
- (29) Michel, J.; Orsi, M.; Essex, J. W. Prediction of Partition Coefficients by Multiscale Hybrid Atomic-Level/Coarse-Grain Simulations. *J. Phys. Chem. B* **2008**, *112*, 657–660.
- (30) Rzepiela, A. J.; Louhivuori, M.; Peter, C.; Marrink, S. J. Hybrid Simulations: Combining Atomistic and Coarse-Grained Force Fields Using Virtual Sites. *Phys. Chem. Chem. Phys.* **2011**, *13*, 10437–10448.
- (31) Heyden, A.; Thrular, J. Conservative Algorithm for an Adaptive Change of Resolution in Mixed Atomistic/Coarse-Grained Multiscale Simulations. *J. Chem. Theory. Comput.* **2008**, *4*, 217–221.
- (32) Masella, M.; Borgis, D.; Cuniasse, P. A Multiscale Coarse-Grained Polarizable Solvent Model for Handling Long Tail Bulk Electrostatics. *J. Comput. Chem.* **2013**, *34*, 1112–1124.
- (33) Neri, M.; Anselmi, C.; Casella, M.; Maritan, A.; Carloni, P. Coarse-Grained Model of Proteins Incorporating Atomistic Detail of the Active Site. *Phys. Rev. Lett.* **2005**, *95*, 218102.
- (34) Riniker, S.; Van Gunsteren, W. F. Mixing Coarse-Grained and Fine-Grained Water in Molecular Dynamics Simulations of a Single System. *J. Chem. Phys.* **2012**, *137*, 044120.
- (35) Pandian, S.; Choi, S. M.; Rhee, Y. M. Simple Method for Simulating the Mixture of Atomistic and Coarse-Grained Molecular Systems. *J. Chem. Theory Comput.* **2013**, *9*, 3728–3739.
- (36) Berendsen, H. J. C.; Postma, J. P. M.; Van Gunsteren, W. F.; Hermans, J. *Intermolecular Forces*; Reidel: Dordrecht, The Netherlands, 1981.
- (37) Darré, L.; Tek, A.; Baaden, M.; Pantano, S. Mixing Atomistic and Coarse Grain Solvation Models for Md Simulations: Let Wt4 Handle the Bulk. *J. Chem. Theory Comput.* **2012**, *8*, 3880–3894.
- (38) Pizzutti, F.; Marchi, M.; Sterpone, F.; Rossky, P. J. How Protein Surfaces Induce Anomalous Dynamics of Hydration Water. *J. Phys. Chem. B* **2007**, *111*, 7584–7590.
- (39) Pomata, M. H.; Sonoda, M. T.; Skaf, M. S.; Elola, M. D. Anomalous Dynamics of Hydration Water in Carbohydrate Solutions. *J. Phys. Chem. B* **2009**, *113*, 12999–13006.
- (40) Laage, D.; Hynes, J. T. A Molecular Jump Mechanism of Water Reorientation. *Science* **2006**, *311*, 832–835.
- (41) Mackerell, A. D., Jr. Empirical Force Fields for Biological Macromolecules: Overview and Issues. *J. Comput. Chem.* **2004**, *25*, 1584–1604.
- (42) Jorgensen, W. L.; Chandrasekaran, R.; Madura, J. D.; Impey, R. W.; Klein, M. L. Comparison of Simple Potential Functions for Simulating Liquid Water. *J. Chem. Phys.* **1983**, *79*, 926–935.
- (43) Berendsen, H. J. C.; Grigera, J. R.; Straatsma, T. P. The Missing Term in Effective Pair Potentials. *J. Phys. Chem.* **1987**, *91*, 6269–6271.
- (44) Guillot, B. A Reappraisal of What We Have Learnt during Three Decades of Computer Simulations on Water. *J. Mol. Liq.* **2002**, *101*, 219–260.

- (45) Ross, S. A.; Sarisky, C. A.; Su, A.; Mayo, S. L. Designed Protein G Core Variants Fold to Native-Like Structures: Sequence Selection by Orbit Tolerates Variation in Backbone Specification. *Protein Sci.* **2001**, *10*, 450–454.
- (46) Hess, B.; Kutzner, C.; Van De Spoel, D.; Lindahl, E. Gromacs 4: Algorithms for Highly Efficient, Load-Balanced, And Scalable Molecular Simulation. *J. Chem. Theory Comput.* **2008**, *4*, 435–447.
- (47) Essman, U.; Perera, L.; Berkowitz, M.; Darden, T.; Lee, H.; Pedersen, L. A Smooth Particle Mesh Ewald Method. *J. Chem. Phys.* **1995**, *103*, 8577–8593.
- (48) Darden, T.; York, D.; Pedersen, L. Particle Mesh Ewald - An N.log(N) Method for Ewald Sums in Large Systems. *J. Chem. Phys.* **1993**, *98*, 10089–10092.
- (49) Hess, B.; Bekker, H.; Berendsen, H. J. C.; Fraaije, J. Lincs: A Linear Constraint Solver for Molecular Simulations. *J. Comput. Chem.* **1997**, *18*, 1463–1472.
- (50) Miyamoto, S.; Kollman, P. A. Settle: an Analytical Version of the Shake and Rattle Algorithm for Rigid Water Models. *J. Comput. Chem.* **1992**, *13*, 952–962.
- (51) Berendsen, H. J. C.; Postma, J. P. M.; Van Gunsteren, W. F.; Dinola, A.; Haak, J. R. Molecular-Dynamics with Coupling to an External Bath. *J. Chem. Phys.* **1984**, *81*, 3684–3690.
- (52) Shirts, M. Simple Quantitative Tests to Validate Sampling from Thermodynamic Ensembles. *J. Chem. Theory Comput.* **2013**, *9*, 909–926.
- (53) Bussi, G.; Donadio, D.; Parrinello, M. Canonical Sampling through Velocity Rescaling. *J. Chem. Phys.* **2007**, *126*, 014101.
- (54) Parrinello, M.; Rahman, A. Polymorphic Transitions in Single Crystals: A New Molecular Dynamics Method. *J. Appl. Phys.* **1981**, *52*, 7182–7191.
- (55) Lindorff-Larsen, K.; Piana, S.; Palmo, K.; Maragakis, P.; Klepeis, J. L.; Dror, R. O.; Shaw, D. E. Improved Side-Chain Torsion Potentials for the Amber Ff99sb Protein Force Field. *Proteins* **2010**, *78*, 1950–1958.
- (56) Van Gunsteren, W. F.; Berendsen, H. J. C. *Gromos-87 Manual*; Biomos Bv: Groeningen, The Netherlands, 1987.
- (57) Martin, O. A.; Vila, J. A.; Scheraga, H. A. Cheshift-2: Graphic Validation of Protein Structures. *Bioinformatics* **2012**, *28*, 1538–1539.
- (58) Vila, J. A.; Arnautova, Y. A.; Martin, O. A.; Scheraga, H. A. Quantum-Mechanics-Derived 13calpha Chemical Shift Server (Che-shift) for Protein Structure Validation. *Proc. Natl. Acad. Sci. U.S.A.* **2009**, *106*, 16972–16977.
- (59) Kell, G. S. Density, Thermal Expansivity, and Compressibility of Liquid Water From 0° to 150° C: Correlations and Tables for Atmospheric Pressure and Saturation Reviewed and Expressed on 1968 Temperature Scale. *J. Chem. Eng. Data* **1975**, *20*, 97–105.
- (60) Neumann, M. Computer Simulation and the Dielectric Constant at Finite Wavelength. *Mol. Phys.* **1986**, *57*, 97–121.
- (61) Ludwig, R. NMR Relaxation Studies in Water-Alcohol Mixtures: The Water-Rich Region. *Chem. Phys.* **1995**, *329*, 329–337.
- (62) Fernandez, D. P.; Mulev, Y.; Goodwin, A. R. H.; Levelt Sengers, J. M. H. A Database for Static Dielectric Constant of Water and Steam. *J. Phys. Chem. Ref. Data* **1995**, *24*, 33–71.
- (63) Eisenberg, D.; Kauzmann, W. *The Structure and Properties of Water*, 2nd ed.; Oxford University Press: Oxford, U.K., 1969.
- (64) Shirts, M. R.; Pande, V. S. Solvation Free Energies of Amino Acid Side Chain Analogs for Common Molecular Mechanics Water Models. *J. Chem. Phys.* **2005**, *122*, 134508.
- (65) Wang, J. H.; Miller, S. Tracer-Diffusion in Liquids. II. The Self-Diffusion as Sodium Ion in Aqueous Sodium Chloride Solutions. *J. Am. Chem. Soc.* **1952**, *74*, 1611–1612.
- (66) Wang, J. H. Tracer-Diffusion In Liquids. III. The Self-Diffusion as Sodium Ion in Aqueous Sodium Chloride Solutions. *J. Am. Chem. Soc.* **1952**, *74*, 1612–1615.
- (67) Tolman, R. C. The Effect of Droplet Size on Surface Tension. *J. Chem. Phys.* **1949**, *17*, 333–337.
- (68) Takahashi, H.; Morita, A. A Molecular Dynamics Study on Inner Pressure of Microbubbles in Liquid Argon and Water. *Chem. Phys. Lett.* **2013**, *573*, 35–40.
- (69) Lei, Y. A.; Bykov, T.; Yoo, S.; Zeng, X. C. The Tolman Length: Is It Positive or Negative? *J. Am. Chem. Soc.* **2005**, *127*, 15346–15347.
- (70) Riniker, S.; Eichenberger, A. P.; Van Gunsteren, W. F. Structural Effects of an Atomic-Level Layer of Water Molecules around Proteins Solvated in Supra-Molecular Coarse-Grained Water. *J. Phys. Chem. B* **2012**, *116*, 8873–8879.
- (71) Arnautova, Y. A.; Vila, J. A.; Martin, O. A.; Scheraga, H. A. What Can We Learn by Computing ¹³C α Chemical Shifts for X-ray Protein Models? *Acta Crystallogr., D. Biol. Crystallogr.* **2009**, *65*, 697–703.
- (72) Cavanagh, J.; Fairbrother, W. J.; Palmer, A. G., III; Rance, M.; Skelton, N. J. *Protein NMR Spectroscopy: Principles and Practice*, 2nd ed.; Academic Press: Amsterdam, 2007.
- (73) Riniker, S.; Van Gunsteren, W. F. A Simple, Efficient Polarizable Coarse-Grained Water Model for Molecular Dynamics Simulations. *J. Chem. Phys.* **2011**, *134*, 084110.
- (74) Roche, J.; Caro, J. A.; Norberto, D. R.; Barthe, P.; Roumestand, C.; Schlessman, J. L.; Garcia, A. E.; Garcia-Moreno, B. E.; Royer, C. A. Cavities Determine the Pressure Unfolding of Proteins. *Proc. Natl. Acad. Sci. U.S.A.* **2012**, *109*, 6945–6950.
- (75) Van Der Spoel, D.; Hess, B. Gromacs - The Road Ahead. *WIREs Comput. Mol. Sci.* **2011**, *1*, 710–715.